IEEE Photonics Journal
An IEEE Photonics Society Publication

Open Access

EWT-ASG: Empirical Wavelet Transform With Adaptive Savitzky–Golay Filtering for TDLAS

Volume 12, Number 3, June 2020

Jianjun He
Cao Song
Qiwu Luo, ***Member, IEEE***
Chunhua Yang, ***Senior Member, IEEE***
Weihua Gui, ***Member, IEEE***

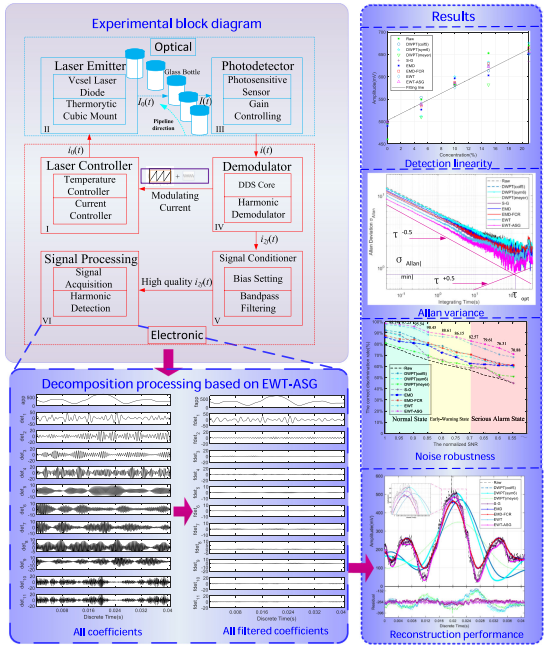

DOI: 10.1109/JPHOT.2020.2992135

EWT-ASG: Empirical Wavelet Transform With Adaptive Savitzky–Golay Filtering for TDLAS

Jianjun He, Cao Song, Qiwu Luo, *Member, IEEE*, Chunhua Yang, *Senior Member, IEEE*, and Weihua Gui, *Member, IEEE*

The School of Automation, Central South University, Changsha 410083, China.

DOI:10.1109/JPHOT.2020.2992135

Manuscript received February 25, 2020; revised April 25, 2020; accepted April 29, 2020. Date of publication May 4, 2020; date of current version May 26, 2020. This work was supported by the National Natural Science Foundation of China under Grant 61873282, Grant 61973323 and Grant 51704089.
Corresponding author: Q. Luo (e-mail: luoqiwu@csu.edu.cn).

Abstract: Inspired by the empirical mode decomposition (EMD)-enhanced gas detection work, this paper develops a further improved signal reconstruction method (namely EWT-ASG) for the demodulated harmonics of tunable diode laser absorption spectroscopy (TDLAS), which is mainly based on empirical wavelet transform (EWT) and Savitzky-Golay (S-G) filtering. First, the imported EWT performs better on the decomposition precision as it successfully bypasses the mode aliasing problem of EMD resulting by the lack of mathematical basis. Second, the improved S-G filter effectively suppresses the noisy components of the wavelet coefficients by updating its one key parameter (i.e., window size w) dynamically according to the correlation coefficients between the raw signals and the decomposed wavelet coefficients. The EWT-ASG scheme was first applied on the oxygen concentration detection for pharmaceutical glass vials. The preliminary experimental results indicate that the EWT-ASG method performs better than recent state-of-the-arts, with an average correct discrimination rate of 98.14% when the normalized SNR is 1. Even when the normalized SNR is degenerated from 1 to 0.85, our detection system still survived well, with a highest average correct discrimination rate of 90.45%. The detection system precision is also improved to a large extent, with a minimal Allan deviation of 0.856@(117s).

Index Terms: Oxygen detection, empirical wavelet transform (EWT), signal reconstruction, open-path optical environment.

1. Introduction

In order to ensure the stability of pharmaceutical ingredients, the measurement of oxygen concentration in pharmaceutical glass vials has become an urgent problem to be solved. With the merits of single-line spectrum analysis, noncontact detection and real-time response in the laboratory [2], [3], [4], [5], the wavelength-modulation-based tunable diode laser absorption spectroscopy (TDLAS/WMS) [1] performs preeminently on the oxygen concentration detection.

Realistically, the oxygen concentration detection device should be carried out under a short-distance and open-path optical condition to adapt to the rapid production of pharmaceutical vials and the special mechanical structure of the production line. Unfortunately, there are diverse interferences in the practical industrial application. Electronic noises inevitably exist in the photoelectric devices. Optical noises such as interference fringes frequently occur on demarcation

surfaces [6], [7]. Environment parameters (e.g., temperature, humidity, pressure, etc) [8] and concentration-independent noises (residual amplitude modulation (RAM)) inherently exist in the detection system [9], [10]. These entangled noises will reduce the signal-to-noise ratio (SNR) of harmonic components [11]. Moreover, in the most cases, the tested oxygen in vials is rarefied (i.e., below 5%) with a short absorbing path, while the outside space is filled with natural oxygen (i.e., 21%) with a relatively long absorbing path. Thus, the useful signal is weak and drowned into these noises.

Therefore, many de-noising methods have been proposed successively. The signal averaging [12], Wiener filter [13], Kalman filter [14] and Wavelet Transform filter [1] have been applied for signal processing in the TDLAS system and improve the precise of the detection. The above filter methods target linear but non-stationary data and non-linear but stationary and deterministic systems. However, the oxygen absorption is a non-linear and non-stationary process with random and non-random noises due to the complex elements existing in the industry filed. Fortunately, Huang *et al.* [15] proposed the empirical mode decomposition (EMD) algorithm, which has been successfully applied to reducing the background noises [16] in TDLAS/WMS system with its excellent performance in processing non-stationary and non-linear signal. Innovatively, Y. Meng *et al.* [17] proposed a modified EMD algorithm in TDLAS/WMS for gas detection, where the harmonic signal was represented with high quality as the distributed noisy components were effectively eliminated by the adaptive signal decomposition framework.

This paper attempts to further the concept of modified EMD based noise suppression method in [17] by importing the empirical wavelet transform (EWT) [18], [19] to address the mode aliasing problem resulted by the lack of mathematical basis in EMD. Meanwhile the Savitzky-Golay filter [20] is improved to suppress the noisy component of the wavelet coefficients by updating its one key parameter dynamically, which enhances the noise robustness. This EWT-ASG algorithm proposed for oxygen concentration detection in pharmaceutical glass vials has achieved good results in experiments.

The rest of this paper is organized as follows. Section 2 presents the EWT-ASG theory. Section 3 introduces the experiment details. Further in Section 4, several actual comparison experiments, noise robustness test, Allan variance analysis and detection linearity are carried out to verify our proposed algorithm. Finally, Section 5 concludes this paper.

2. Principles of EWT-ASG

EWT, a new method to build adaptive wavelets, is capable of extracting the different modes of a signal by designing an appropriate wavelet filter bank. Compared with its predecessor EMD, EWT not only avoids the mode aliasing, but also can accurately extract intrinsic mode functions (IMFs) from noise environment. Moreover, EWT based on the wavelet framework can adaptively select the number of decomposition levels. Therefore, EWT is crucially adapted in the signal reconstruction. The working process of signal reconstruction can be divided into five main parts: Firstly, the raw 2nd harmonic signal $f(k)$ is decomposed into all possible detail coefficients and approximation coefficient. Secondly, the cross-correlation coefficients C_i between $f(k)$ and detail coefficients and the C_1 between $f(k)$ and approximation coefficient are obtained by cross-correlation operation, respectively. Thirdly, the parameter of Savitzky-Golay filter is updated adaptively. Fourthly, all coefficients are filtered by the Savitzky-Golay filter, then, we obtain the filtered coefficients. Finally, the 2nd harmonic signal is reconstructed by inverse empirical wavelet transform (IEWT). The detailed steps are presented as follows:

Step 1. A total of $n-1$ local maxima values in the normalized Fourier spectrum of raw 2nd harmonic signal $f(k)$ are detected based on automatic detection of the number of modes, and then, these maxima values are sorted in decreasing order (0 and π are excluded), thus, $f(k)$ is segmented into n segments in the frequency range $[0, \pi]$ according to the $n+1$ boundaries (the specific process can be referred in [18]). ω_{n} denotes the central frequency of each segment (see Fig. 1). Centered around each ω_{n}, a transition phase (the gray hatched areas in Fig. 1) T_{n} of spectrum width $2\tau_{\mathrm{n}}$ is defined.

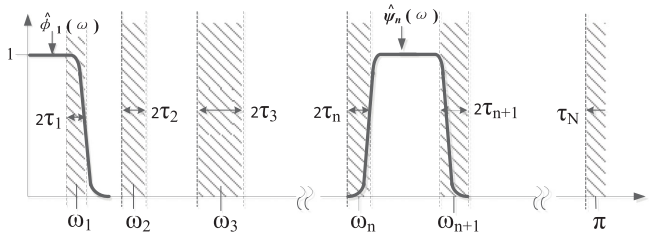

Fig. 1. Partitioning of the Fourier axis.

Step 2. The signals after passing through filters are obtained by the inner products of scaling function and empirical wavelets with raw 2nd harmonic signal. Concretely, the empirical scaling function (lowpass filter) and empirical wavelet (bandpass filter) can be expressed by (1) and (2), respectively.

$$\hat{\phi}_n(\omega) = \begin{cases} 1 \, if \, |\omega| \le (1-\gamma)\,\omega_n \\ \cos\left[\frac{\pi}{2}\beta\left(\frac{1}{2\gamma\omega_n}\left(|\omega| - (1-\gamma)\,\omega_n\right)\right)\right] \\ if \, (1-\gamma)\,\omega_n \le |\omega| \le (1+\gamma)\,\omega_n \\ 0 \quad \text{otherwise} \end{cases} \tag{1}$$

$$\hat{\psi}_n(\omega) = \begin{cases} 1 \, if \, (1+\gamma)\,\omega_n \le |\omega| \le (1-\gamma)\,\omega_{n+1} \\ \cos\left[\frac{\pi}{2}\beta\left(\frac{1}{2\gamma\omega_{n+1}}\left(|\omega| - (1-\gamma)\,\omega_{n+1}\right)\right)\right] \\ if \, (1-\gamma)\,\omega_{n+1} \le |\omega| \le (1+\gamma)\,\omega_{n+1} \\ \sin\left[\frac{\pi}{2}\beta\left(\frac{1}{2\gamma\omega_n}\left(|\omega| - (1-\gamma)\,\omega_n\right)\right)\right] \\ if \, (1-\gamma)\,\omega_n \le |\omega| \le (1+\gamma)\,\omega_n \\ 0 \quad \text{otherwise} \end{cases} \tag{2}$$

Where, $\tau_n = \gamma\omega_n (0 < \gamma < 1, \gamma < \min \frac{\omega_{n+1}-\omega_n}{\omega_{n+1}+\omega_n})$and the function $\beta(x)$ is

$$\beta(x) = x^4(35 - 84x + 70x^2 - 20x^3) \tag{3}$$

Then, the signal (approximation coefficient) after passing through lowpass filter is given by the inner product with the scaling function:

$$W_f^{\varepsilon}(0, k) = \langle f(k), \phi_1(k) \rangle = F^{-1}\left[f(\omega)\hat{\phi}_1(\omega)\right] \tag{4}$$

and the signal (detail coefficient) after passing through bandpass filter is given by the inner products with the empirical wavelets:

$$W_f^{\varepsilon}(n, k) = \langle f(k), \psi_n(k) \rangle = F^{-1}\left[f(\omega)\hat{\psi}_n(\omega)\right], (n \ge 1) \tag{5}$$

where, k is the number of discrete points in a 2nd harmonic signal.

Step 3. The cross-correlation coefficient C_n between $f(k)$ and $W\varepsilon\ f(n, k)$ is calculated by using cross-correlation operation, as follows:

$$C_n = \frac{1}{k}\sum_{i=1}^{k} f(k) \bullet fW_f^{\varepsilon}(n, k) \tag{6}$$

Step 4. The window size w of Savitzky-Golay filter is updated adaptively. If the sum of C_i ($2 \le i \le n$) in this time is less than that in the last time, which indicates the noise fluctuation is larger in this time, the w needs to be broadened and we set $w = w/C_1$. Otherwise, the w should to be narrowed down, which is set $w = w \cdot C_1$.

Step 5. The coefficients $W\varepsilon\ f(n, k)$ are filtered by using the Savizky-Golay algorithm to obtain the filtered coefficients $fW\varepsilon\ f(n, k)$.

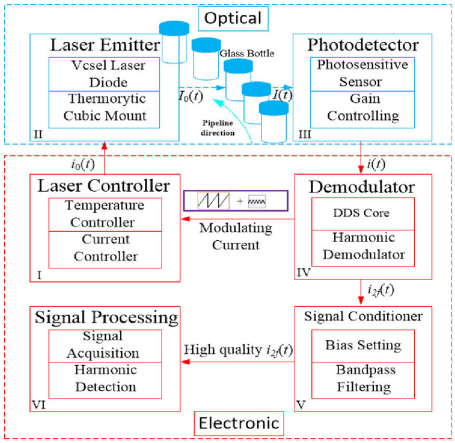

Fig. 2. Experimental block diagram of oxygen concentration detection for pharmaceutical glass vials.

Step 6. The filtered coefficients $fW\varepsilon\ f(n, k)$ are set the weight, the weighted signal can be expressed by (7).

$$W_f^{\varepsilon}(n, k) = C_n \bullet fW_f^{\varepsilon}(n, k) \tag{7}$$

Step 7. The reconstructed 2nd harmonic signal can be obtained by IEWT

$$f(k) = W_f^{\varepsilon}(0, k) \bullet \phi_1(k) + \sum_{n=1}^{N} W_f^{\varepsilon}(n, k) \bullet \psi_n(k) \tag{8}$$

The above steps constitute signal reconstructor. After the processing of the steps 1–7, we can obtain the reconstructed 2nd harmonic signal used for oxygen concentration detection subsequently.

3. Experiment Details

The experimental block diagram of oxygen concentration detection for pharmaceutical glass vials are designed, which consists of two main parts. As shown in Fig. 2, the laser emitter (II, Laser component, single mode VCSEL, 760 nm, TO5 footprint) conducts at a stationary temperature in conjunction with the laser controller (I, Thorlabs, VITC002), and its current controller is controlled by the DDS core of the demodulator (IV), which generates a modulated current to actuate the laser diode. The photodetector (III, Thorlabs, PDA36A, 350–1100 nm) receives the transmission intensity of the laser beams traveling through the open-path optical path, which is by phase-lock demodulated in the digital demodulator (IV), then the modulated spectrum absorbed by O_2 can be extracted. The band-limited signal regulator (V) amplifies the weak 2nd harmonic signal after demodulation, setting the bandwidth to 0.01 Hz $\sim$ 150 Hz for noise-robustness reduction. Feature extraction and calculation are completed by signal processing unit (VI), which is a crucial factor in oxygen concentration inversion and pharmaceutical glass vial qualification determination. Here we applied the designed TDLAS/WMS prototype on an automated visual inspection (AVI) machine (Truking Tech., AJDZ48A show in Fig. 3), where our proposed EWT-ASG algorithm will be carried out and verified. It is worth to mention that the parameters and configurations of this prototype are the same as our previous work [1] and the temperature range in the workshop is 25 °C to 32 °C.The raw 2nd harmonics of 0% oxygen concentration for pharmaceutical glass bottle are obtained, taking one of the raw 2nd harmonics as an example for subsequent analysis and discussion, then a 2nd harmonic $f(k)$ is shown in Fig. 4 (black dashed line).

Through the theoretical analysis in steps 1–3, the obtained coefficients of $f(k)$ are shown in Fig. 5. In this paper, we particularly segment $f(k)$ into eleven segments and the corresponding

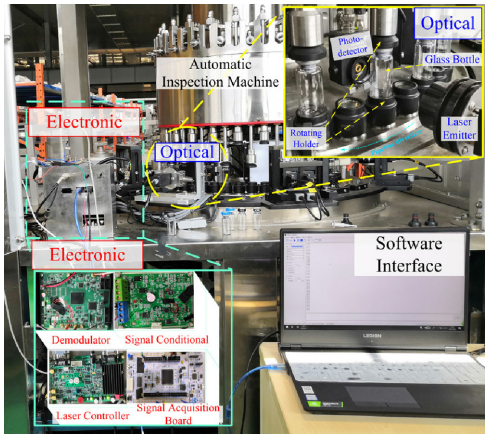

Fig. 3. Experiment platform of oxygen concentration detection for pharmaceutical glass vials.

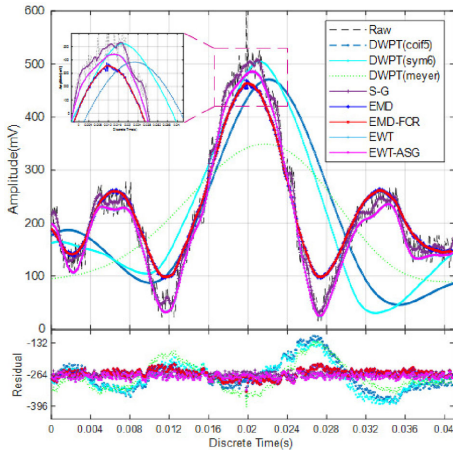

Fig. 4. Filtered 2nd harmonics and its corresponding residuals by using different methods.

central frequency are 0.1841, 0.5645, 0.7854, 1.0308, 1.5340, 1.6812, 1.8285, 1.9758, 2.1230, 2.2948, 2.6753, respectively. The $f(k)$ is decomposed into 12 coefficients (including 1 approximation coefficient and 11 detail coefficients) and the frequency band of each coefficient is between ω_{n} and $\omega_{\mathrm{n+1}}$ mentioned in step 1. As can be seen from Fig. 5, the approximation coefficient is flat and smooth, which is the most similar to the raw signal. With the increasing of decomposition layer, the fluctuation of the detail coefficient becomes more and more violently, which contains more high-frequency components. And it is interesting to note that the decomposition layer of each 2nd harmonic signal maybe different due to the characteristics of difference in oxygen concentration and multiple stochastic noises superimposed on the 2nd harmonic signal. Fortunately, this decomposition processing has a strong self-adaptability and is suitable for the effective decomposition of 2nd harmonic signals with unknown oxygen concentration, because it automatically selects the decomposition layers according to the segmented frequency mentioned in step 1. Through steps 4–7, the obtained filtered coefficients of the $f(k)$ and the reconstructed signal are shown in Fig. 6. Particularly in this paper, the correlation coefficients C_1 to C_{12} are 0.9869, 0.0936, -0.0349, 0.0195, -0.0264, 0.0256, 0.0152, -0.0272, -0.0214, 0.0306, -0.0308, 0.0200, respectively. It indicated that approximation coefficient has the highly correlation degree with the $f(k)$, while other detail coefficients have lowly correlation degree. So, the principal components in $f(k)$ can be

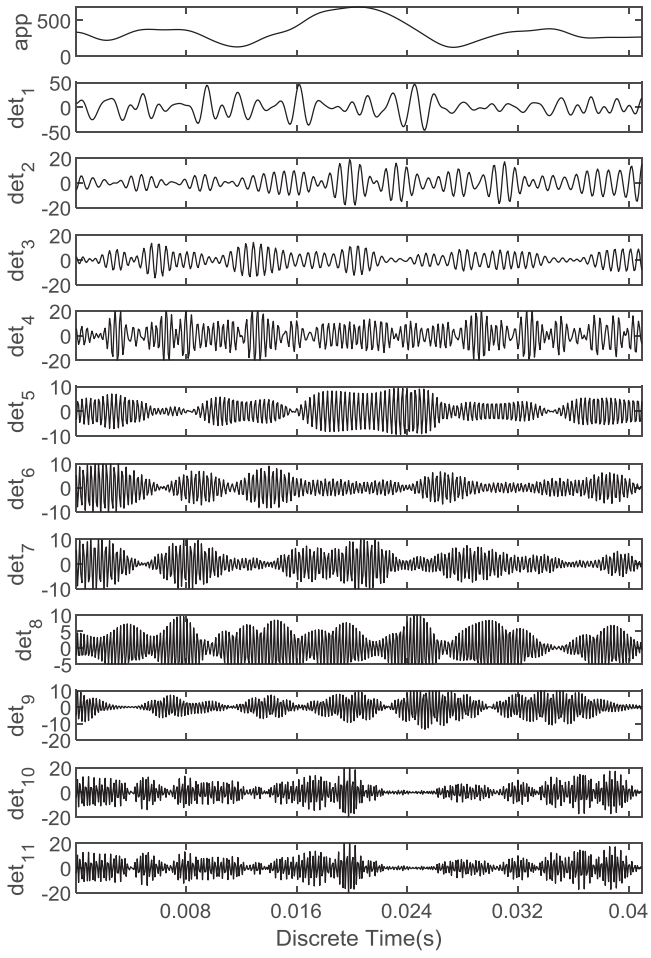

Fig. 5. All coefficients by EWT of a 2nd harmonic signal with 0% oxygen concentration for glass pharmaceutical vial.

automatically enhanced and other nonsignificant components can be weakened by reconstruction couple with cross-correlation operation.

4. Results

4.1 Signal Reconstruction Performance

Different filtering methods are compared in Fig. 4 to show the performance of our proposed SWT-ASG algorithm. To be consistent with the Reference [1], which used discrete-time wavelet packet transform (DWPT) with different mother wavelet functions to generate the signal reconstructor, we choose the same three typical wavelet functions of Coiflets, Symlets and Meyer as mother wavelet function, where the amplitude drop is in accord with the result in [1] when using Meyer. As the waveform of Meyer has a considerable discrepancy with the ideal 2nd harmonic, the result of the convolution of the raw 2nd signal with the infinite impulse response filter can not fit the symmetric 2nd harmonic well. Inversely, the waveform of others mother wavelet (eg. Coiflets, Symlets) have small amplitude attenuation with the property describing the raw principal trend well. It is worth mentioning that the reconstructed 2nd harmonic by DWPT cannot reach the quality of the filtered signal shown in [1], for the reason that DWPT can hardly extract the main signal from the more complex noises existing in the industry field, such as the constant pulse interference

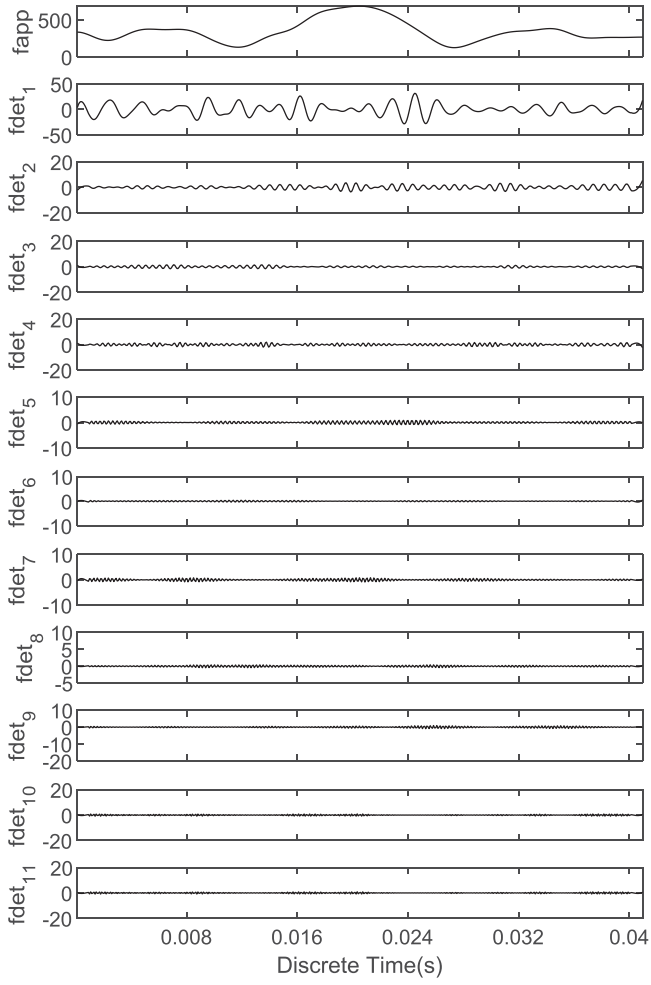

Fig. 6. All filtered coefficients by EWT of a 2nd harmonic signal 0% oxygen concentration for glass pharmaceutical vial.

coming from the power grid and the stochastic high frequency noises superimposed on the 2nd harmonic. It can be clearly observed that, when using EMD method [16], the amplitude of the reconstructed signal drops slightly and this signal is still not so symmetric, which mainly caused by that mode aliasing easily generates between different modes, leading to the principle feature cannot be effectively extracted from each mode. Furthermore, the EWT well resolves this mode aliasing problem of EMD resulting by the lacking mathematical basis and it can reconstruct the 2nd harmonic relatively accurately. The S-G filter using the least squares fitting coefficient as filter response function can suppress the high frequency noise to some extent. The EMD-based method combining Savitzky-Golay filter, cross-correlation and signal re-construction (EMD-FCR) [17] improves the SNR a bit comparing to the EMD scheme. As expected, our proposed EWT-ASG performs the bright effect. Notably, it not only suppresses the random noises but also maintains the symmetry of the waveform. We define the fidelity, a cross-correlation coefficient between the raw 2nd harmonic and filtered 2nd harmonic. As shown in Table I. S-G, EMD, EMD-FCR, EWT and EWT-ASG have high fidelity. The residual value and the operation time (calculating by MATLAB for fair comparison) of filtered 2nd harmonic using S-G is lowest (shown in Table I) as the simple average fitting based on sliding window without complex mathematical processing and the ability of rapid time response. Moreover, the operation time of EWT-ASG is supposed to be accelerated under the condition of decent fidelity and considerable residuals. It is also worth mentioning that the

TABLE I
Quantitative Comparison of Different Methods On 2nd Harmonics

Methods	Fidelity	Average absolute residual (mV)	Operation time (s)	Average absolute deviation	The correct discrimination rate (%) SNR=1	SNR=0.55	$\sigma_{Allan}@\tau_{opt}$(s)	MDL (%)	R^2
Raw	-	-	-	13.43	79.35	45.25	1.933@(124s)	6.21	0.9413
DWPT(coif5)[1]	0.6042	21.97	0.1437	10.45	92.22	60.14	1.830@(129s)	2.01	0.9835
DWPT(sym6)[1]	0.6673	17.15	0.1547	10.93	90.45	58.97	1.870@(130s)	4.25	0.9562
DWPT(meyer)[1]	0.5132	23.36	0.1242	7.87	80.70	50.85	1.916@(119s)	3.41	0.9435
S-G[20]	**0.9907**	**0.022**	**0.0069**	6.10	90.72	44.91	1.920@(115s)	4.66	0.9434
EMD[16]	0.9821	5.43	0.0319	8.78	86.00	60.99	1.459@(102s)	3.59	0.9540
EMD-FCR[17]	0.9795	5.56	0.0534	7.52	87.31	61.00	1.280@(112s)	2.08	0.9905
EWT[18]	0.9887	19.34	0.0397	6.73	97.13	68.04	1.132@(109s)	2.64	0.9868
EWT-ASG	0.9876	19.33	0.0666	**3.24**	**98.14**	**70.88**	**0.856@(117s)**	**1.01**	**0.9939**

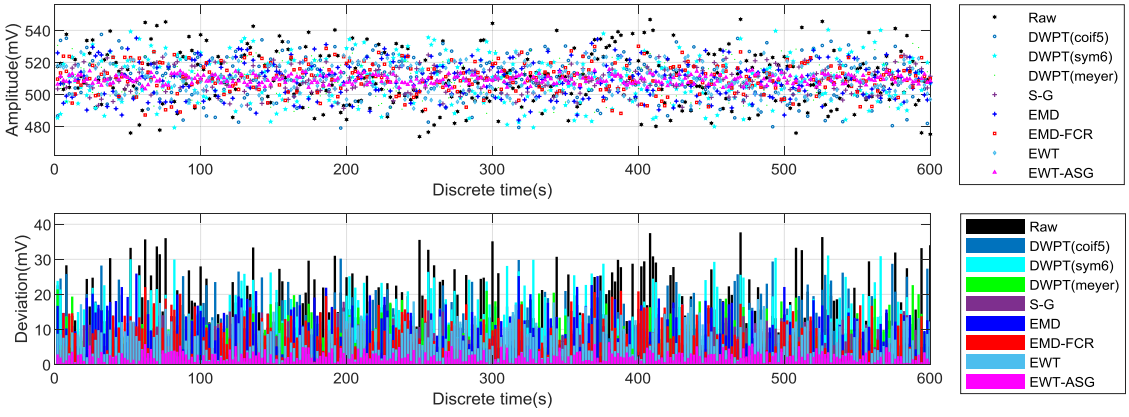

Fig. 7. The $V_{P\text{-}P}$ and absolute deviation of 2nd harmonic of 0% oxygen concentration for glass pharmaceutical vial for 600 s.

positive correlation degree of approximation coefficient for general 2nd harmonic signal is higher than that of other detail coefficients, and the principle components of most 2nd harmonic signals may concentrate at low frequency band.

4.2 Detection Stability

In order to verify the detection stability of our proposed methods, we go on with a series of experiments. Here, the glass vials with oxygen concentration value of 0% are chosen as the test samples and detected for 10min. Each 2nd harmonic is processed by using the methods mentioned in the Sec. IV. A. The peak-to-peak values ($V_{p\text{-}p}$) of successive 2nd harmonics using various filtering methods are extracted as shown in upper part of Fig. 7. Here, the absolute deviation is defined as the absolute value of difference between the average value of all $V_{p\text{-}p}$ and a single $V_{p\text{-}p}$ to verify the stability performance under different methods, as shown in bottom part of Fig. 7. It can be seen

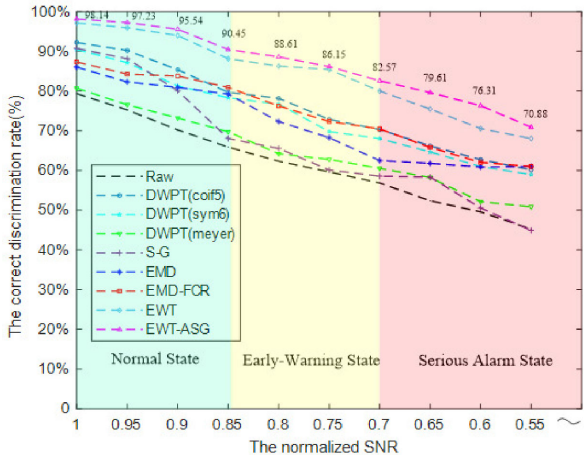

Fig. 8. Correct discrimination rate by using the different methods for standard glass vials with 5% oxygen concentration when the SNR decreases successively.

from Table I that EWT-ASG has the minimum average absolute deviation, which verifies the optimal property of this method again. Moreover, our system can run stably for a period of time under the condition of ensuring a certain detection accuracy, which puts a solid engineering foundation for the implementation in the industrial field in the future.

4.3 Noise Robustness

Here, in order to evaluate the noise robustness of our proposed method, plentiful of comparative tests are carried out. The 300 2nd harmonic signals from standard glass vials with 0% and 5% oxygen concentrations are acquired, respectively. Then, the Gaussian white noises with different normalized SNRs are superimposed on these raw 2nd harmonic signals. As shown in Fig. 8, three states for oxygen concentration detection system are defined respectively: normal state ($0.85 < \text{SNR} \leq 1$), early-warning state ($0.7 \leq \text{SNR} \leq 0.85$), and serious alarm state (SNR <0.7). For glass vials with 0% and 5% oxygen concentration, the $V_{\text{p-p}}$ of all 2nd harmonic signals with different SNRs was extracted. Then, we take the threshold defined in the Reference [1] as the criterion of correct or fault discrimination, which is the average of the maximum of 300 $V_{\text{p-p}}$ of 2nd harmonic signals of glass vial with 0% oxygen concentration and the minimum of 300 $V_{\text{p-p}}$ of 2nd harmonic signals of glass vial with 5% oxygen concentration. Thus, these correct discrimination rates of 5% oxygen concentration are shown in Fig. 7 and the correct discrimination rates by using different methods are presented in Table I when the SNR is set to 1 and 0.55, respectively. The rose red dashed line in Fig. 8 is the correct discrimination rate curve with EWT-ASG. The correct discrimination rate of the method of EWT-ASG is higher than 90% when the SNR is in the range of first state, while that of other schemes are slippery slope, which shows the EWT-ASG achieves the best performance in terms of noise-robust. Sequentially, the correct discrimination rates of all methods degenerate gradually with the increase of noises during the second state; however, the value of 70.88% (SNR $=$ 0.55) represents that the EWT-ASG method can still overcomes some noises in this state, though this value is closed to serious alarm limit. The last state is a terrible situation to this detection system and it rarely happens. These above-mentioned results prove that the EWT-ASG method works efficaciously when the normalized SNR ranges in [0.85, 1].

4.4 Allan Variance Analysis

The Allan variance analysis of different methods is carried out to identify the different noise terms and calculate the detection limit of the sensor in the time domain [21], [22], here, 22500 2nd

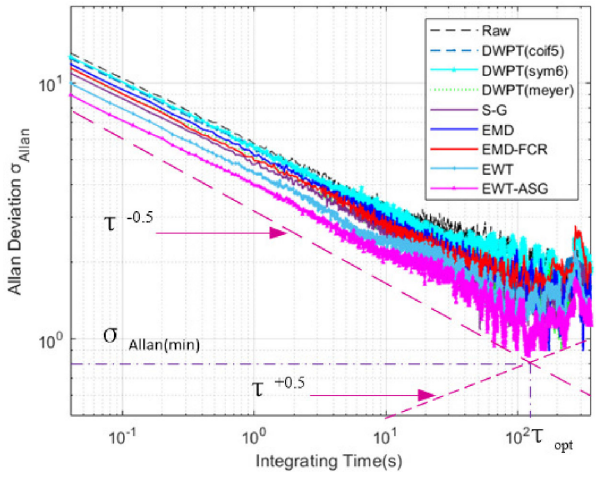

Fig. 9. Allan plots of different methods for the standard glass vials with 0% oxygen concentration.

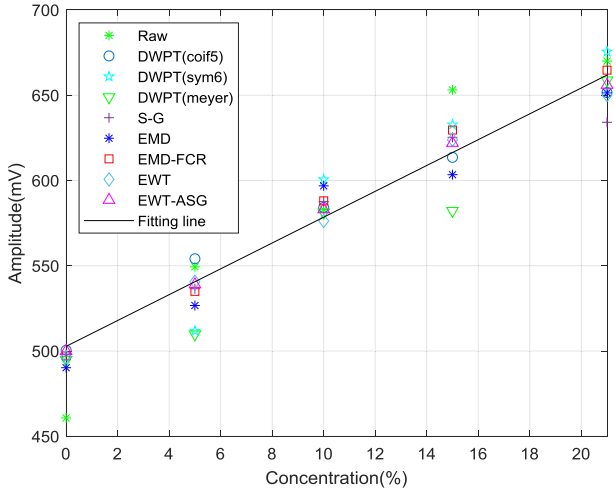

Fig. 10. The relationship between $V_{p\text{-}p}$ and oxygen concentration.

harmonics are acquired from the glass bottles with 0% oxygen concentration for measuring 15min. The Allan variance (σ_{Allan}) analysis results with the different methods are shown in Fig. 9. The white noise is dominant when the slope is -0.5 (dashed line) and the Brownian noise is dominant when the slope is 0.5 (dotted line) [23], [24]. This Figure shows that the measurement precision by taking the EWT-ASG method is higher than that of other methods both in the white and Brownian noise range. The method of EWT-ASG can obtain the lowest minimum σ_{Allan} ($\sigma_{\mathrm{Allan(min)}}$) for 0% oxygen concentration glass vial among different methods from the Table I, concretely. These results proved that precision of our detection system coupled with EWT-ASG method. Therefore, these experimental results above provide a solid theoretical basis for the application of our method in the field of oxygen concentration detection in the industrial environment.

4.5 Detection Linearity

To further verify the performances of the EWT-ASG method, we performed the different oxygen concentrations detection experiment for 1min. We prepared five distinct pharmaceutical glass vials with oxygen concentrations of 0%, 5%, 10%, 15% and 21% by using the oxygen-nitrogen mixing

method, then, the average value of all $V_{p\text{-}p}$ of 2nd harmonics for a certain glass vial are obtained as shown in Fig. 10. It can be seen that the relationship between the average $V_{p\text{-}p}$ and oxygen concentration is linear with the slope of 7.574 mV/% by using EWT-ASG. The results of the linear correlation coefficient R^2 are shown in Table I, which presents the highest R^2 of 0.9939 using EWT-ASG method. Then, the minimum detection limit (MDL) [17] is defined as follows:

$$MDL = \frac{1}{K} \bullet 2A_{noise} \tag{9}$$

Where A_{noise} is the amplitude of the noises, and K is the slope of the fitting line. Thus, the MDLs of the raw 2nd harmonic signal and filtered signal based on different methods are obtained when the normalized SNR is 1 as shown in Table I. Therefore, the EWT-ASG method can improve the detection linearity and detection limit. Moreover, the EWT-ASG method can also be used for other non-stationary and non-linear signal processing.

5. Conclusions

This paper focuses on how to build a noise robustness signal reconstruction method for TDLAS system in the open-path environment. Aiming at the weak demodulated harmonic signal for the oxygen concentration detection of pharmaceutical vials under a short-distance and open-path optical industry condition, the EWT-based signal decomposition scheme and the adaptive S-G filter are designed to improve the SNR of reconstructed harmonic signal. Taking AVI machine equipped in *Truking Tech*. as a test bench, our EWT-ASG method was preliminary evaluated on our pervious designed TDLAS/WMS prototype and delightfully achieved minimum average absolute detection deviation and superior anti-noise robustness compared with previous signal filtered methods. However, several improving points should be urgently taken in the near future: Filter algorithm and concentration inversion algorithm need to be fused to further improve the accuracy of oxygen concentration discrimination. The calculation speed of the EWT-ASG method should be taken to catch up with the average production speed of 400 vials per minute. In conclusion, we hope this preliminary work will contribute to the development of on-line oxygen concentration detection a bit and provide some inspiration for others.

References

[1] Q. Luo *et al.*, "Headspace oxygen concentration measurement for pharmaceutical glass vials in open-path optical environment using TDLAS/WMS," *IEEE Trans. Instrum. Meas.*, DOI: 10.1109/TIM.2019.2958582, Dec. 2019.
[2] Y. Ding *et al.*, "Half-width integral method for gas concentration measuring in tunable diode laser absorption spectroscopy," *Spectrosc. Lett.*, vol. 46, no. 7, pp. 465–471, Jun. 2013.
[3] Y. Du and Z. Peng, Y. Ding, "Wavelength modulation spectroscopy for recovering absolute absorbance," *Opt. Express*, vol. 26, no. 7, pp: 9263–9272, 2018.
[4] A. Upadhyay, D. Wilson, M. Lengden, A. L. Chakraborty, G. Stewart, and W. Johnstone, "Calibration-Free WMS Using a cw-DFB-QCL, a VCSEL, and an Edge-Emitting DFB laser with in-situ real-time laser parameter characterization," *IEEE Photonics J.*, vol. 9, pp. 1–17, 2017.
[5] Y. Xie *et al.*, "A DFB-LD internal temperature fluctuation analysis in a TDLAS system for gas detection," *IEEE Photonics J.*, 11, pp. 1–8, (2019).
[6] D. T. Cassidy and J. Reid, "Harmonic detection with tunable diode lasers two-tone modulation," *Appl. Phys. B*, vol. 29, pp. 279–285, 1982.
[7] L. Persson, F. Andersson, M. Andersson, and S. Svanberg, "Approach to optical interference fringes reduction in diode laser absorption spectroscopy," *Appl. Phys. B*, vol. 87, no. 3, pp. 523–530, May. 2007.
[8] W. Liang, Q. Zhou, X. Dong, and T. Lv, "Influence of temperature induced cavity length variation in wavelength modulation spectroscopy," *Optik*, vol. 172, pp. 220–224, 2018.
[9] J. T. C. Liu, J. B. Jeffries, and R. K. Hanson, "Wavelength modulation absorption spectroscopy with 2f detection using multiplexed diode lasers for rapid temperature measurements in gaseous flows," *Appl. Phys. B*, vol. 78, no. 3–4, pp. 503–511, 2004
[10] I. Daubechies, J. Lu, and H. Wu, "Synchrosqueezed wavelet transforms: An empirical mode decomposition-like tool," *Appl. Comput. Harmon. A.*, 30, pp. 243–261, 2011.
[11] H. Riris, C. B. Carlisle, R. E. Warren, and D. E. Cooper, "Signal-to-noise ratio enhancement in frequency-modulation spectrometers by digital signal processing," *Opt. Lett.*, vol. 19, no. 2, pp. 144–146, Jan. 1994.

[12] P. Werle, R. Mücke, and F. Slemr, "The limits of signal averaging in atmospheric trace-gas monitoring by tunable diodelaser absorption spectroscopy (TDLAS)," *Appl. Phys. B*, vol. 57, no. 2, pp. 131–139, Aug. 1993.
[13] P. Werle, B. Scheumann, and J. Schandl, "Real-time signal-processing concepts for trace-gas analysis by diodelaser spectroscopy," *Opt. Eng.*, vol. 33, no. 9, pp. 3093–3105, Sep. 1994.
[14] D. P. Leleux, R. Claps, W. Chen, F. K. Tittel, and T. L. Harman, "Applications of Kalman filtering to real-time trace gas concentration measurements," *Appl. Phys. B*, vol. 74, no. 1, pp. 85–93, Jan. 2002.
[15] N. E. Huang *et al*., "The empirical mode decomposition and the Hilbert spectrum for nonlinear and non-stationary time series analysis," *Proceedings A*, vol. 454, no. 1, pp. 903–995, 1998.
[16] R. Yang, Y. Bi, Q. Zhou, X. Dong, and T. Lv, "A background reduction method based on empirical mode decomposition for tunable diode laser absorption spectroscopy system," *Optik*, 158, pp. 416–423, 2018.
[17] Y. Meng, T. Liu, K. Liu, J. Jiang, R. Wang, T. Wang, and H. Hu, "A modified empirical mode decomposition algorithm in TDLAS for gas detection," *IEEE Photonics J.*, 6, pp. 1–7, (2014).
[18] J. Gilles, "Empirical wavelet transform," *IEEE Trans. Signal Process*, vol. 61, no. 16, pp. 3999–4010, Aug. 2013.
[19] S. N. Chegini, A. Bagheri, and F. Najafi, "Application of a new EWT-based denoising technique in bearing fault diagnosis," *Measurement*, vol. 144, pp. 275–297, Oct. 2019.
[20] A. Savitzky and M. J. E. Golay, "Smoothing and differentiation of data by simplified least squares procedures," *Anal. Chem*., vol. 36, no. 8, pp. 1627–1639, Jul. 1964.
[21] D. W. Allan, "Statistics of atomic frequency standards," *Proc. IEEE*, vol. 54, no. 2, pp. 221–230, Feb. 1966.
[22] P. Werle, R. Mücke, and F. Slemr, "The limits of signal averaging in atmospheric trace-gas monitoring by tunable diode-laser absorption spectroscopy (TDLAS)," *Appl. Phys. B*, vol. 57, no. 2, pp. 131–139, 1993.
[23] L. Lan, J. Chen, X. Zhao, and H. Ghasemifard, "VCSEL-Based atmospheric trace gas sensor using first harmonic detection," *IEEE Sensor. J.*, vol. 19, no. 13, pp. 4923–4931, Jun. 2019.
[24] L. Lan, J. Chen, Y. Wu, Y. Bai, X. Bi, and Y. Li, "Self-calibrated multiharmonic CO2 sensor using VCSEL for urban in situ measurement," *IEEE Trans. Instrum. Meas.*, vol. 68, no. 4, pp. 1140–1147, Apr. 2019.